Engineered Regeneration 6 (2025) 133–145

Contents lists available at ScienceDirect

Engineered Regeneration

journal homepage: http://www.keaipublishing.com/en/journals/engineered-regeneration/

Force induces axon growth in inhibitory conditions

Elena Capitanini[a,1], Laura Talarico[a,1], Sara De Vincentiis[a], Chiara Giacomelli[b], Sara Vitolo[a], Lorenzo Da Palmata[a], Laura Marchetti[b], Elisabetta Ferraro[a], Maria Letizia Trincavelli[b], Vittoria Raffa[a,*]

[a] Dipartimento di Biologia, Università di Pisa, Pisa 56126, Italy
[b] Dipartimento di Farmacia, Università di Pisa, Pisa 56126, Italy

ARTICLE INFO

Keywords:
Mechanical force
Axon growth
Regeneration
Inhibition
Inflammation

ABSTRACT

Axon navigation is guided by spatial patterns of chemical and physical cues in the developing central nervous system. Following injury, these patterns are disrupted, the microenvironment evolves rapidly, and inhibitory molecules create a barrier to the regeneration of severed axons. We have recently developed a technology called nano-pulling designed to stimulate axon growth and regeneration by modulating neuronal mechanotransduction. In this paper, we demonstrate that nano-pulling can induce axon growth in hippocampal neurons even in the presence of repulsive cues, such as chondroitin sulfate proteoglycans, semaphorin 3A, microglial activation, and pro-inflammatory cytokines. Nano-pulling can also enhance the elongation of neural processes in neural progenitors transplanted into an organotypic spinal cord injury model that mimics the tissue complexity and inflammation seen in *in vivo* models. Our data suggest that nano-pulling could be used as a strategy to manipulate axon growth, overcoming certain extrinsic inhibitory factors.

1. Introduction

The microenvironment profoundly influences the regenerative capacity of neurons within the central nervous system (CNS) [1]. The absence of axonal regeneration does not stem from an intrinsic limitation of the CNS; rather, it arises from variations in the microenvironment, which is significantly more permissive in the peripheral nervous system (PNS) compared to the CNS [2]. Various inhibitory molecules contribute to the negative modulation of axon growth [3,4]. For example, the neuroinflammation elicited by activated astrocytes and microglial cell significantly impedes axonal regeneration of the retracted neuronal processes [5]. Key molecules with anti-regenerative properties secreted by these cells includes chondroitin sulfate proteoglycans, semaphorins, and myelin-associated inhibitors. Among these, chondroitin sulfate proteoglycans (CSPGs) have been the subject of extensive investigation. CSPGs are constituents of the extracellular matrix, predominantly secreted by reactive glial cells. In cultured neurons, CSPGs inhibit neurite outgrowth [6]. Following CNS injuries, upregulated CSPGs at the lesion site create an inhibitory barrier that obstructs the regeneration of severed axons [7]. Furthermore, while the inhibitory effects of CSPGs are well-established, their activity becomes increasingly complex when they act in concert with other molecules, such as semaphorins and myelin-associated inhibitors [8]. Semaphorins were initially identified in the context of axon guidance [9]; however, subsequent research has unveiled diverse roles for these molecules. For instance, semaphorin 3A (Sema-3A) has been shown to repel axon growth across multiple systems, including axons from the dorsal root ganglia [10], cortical axons [11], hippocampal axons [12], and cerebellar axons [13] via neuropilin-plexin receptor complexes [14].

Neuroinflammation and the inhibitory environment associated with CNS injuries are critical determinants of axonal degeneration [15]. Pro-inflammatory microglial cells and recruited macrophages actively contribute to axonal retraction by phagocytizing damaged synapses and retracting processes. Concurrently, reactive astrocytes produce CSPGs, thereby establishing an inhibitory gradient that exacerbates axonal retraction and growth cone collapse [16]. Despite the initiation of certain regenerative efforts, the existence of a non-permissive pro-inflammatory and inhibitory microenvironment hinders significant process elongation, rendering the restoration of functional circuitry through intrinsic regenerative capacity alone a distant goal. Thus, it becomes imperative to employ therapeutic strategies that facilitate process elongation by surmounting the adversities of the microenvironment and/or in conjunction with treatments aimed at ameliorating the inflammatory-inhibitory state [17–19].

Peer review under the responsibility of KeAi Communications Co., Ltd
* Corresponding author.
E-mail address: vittoria.raffa@unipi.it (V. Raffa).
[1] Equally contributing

https://doi.org/10.1016/j.engreg.2025.05.003
Received 20 January 2025; Received in revised form 29 May 2025; Accepted 30 May 2025
Available online 6 June 2025

In the realm of regenerative therapy, magnetic nanoparticles (MNPs) have attracted considerable attention in recent years for their promising potential as a modality to promote axon regeneration through mechanical stimulation [20]. This technique, termed nano-pulling, capitalizes on the capability of MNPs to be internalized into the axoplasm and to generate a dragging force under the influence of an external static magnetic field [21]. Nano-pulling produces exogenous low-intensity traction forces on axons (about 10 pN) [22], which are likely the most potent inducers of axon growth described so far. This approach has been observed to double the rate of axon elongation while halving the time required for synaptic maturation in primary hippocampal neurons [21,23]. Following axotomy of dorsal root ganglia, nano-pulling doubles the rate of axon regeneration without the addition of any growth factors [24]. Moreover, nano-pulling also accelerates the differentiation of neural progenitors into mature neurons [25]. More specifically, active mechanical stimuli can promote the differentiation of neural progenitors transplanted into spinal cord (SC) tissue into mature neurons and guide the elongation of their processes. This groundbreaking discovery presents new avenues for enhancing the efficacy of cell replacement therapies.

In this context, we seek to address the question of whether nano-pulling can modulate axon growth in the presence of an inhibitory microenvironment, effectively bypassing or overcoming the influence of these extrinsic inhibitory factors. We aim to validate this hypothesis using primary hippocampal neurons subjected to various inhibitory stimuli (inflammation, chondroitin sulfate proteoglycans, semaphorins). Ultimately, we have developed an *ex vivo* model of inflammation to test nano-pulling on neural progenitors transplanted in the SC tissue.

2. Experimental section/methods

2.1. Ethical statements

Animal procedures were performed in strict compliance with protocols approved by Italian Ministry of Public Health and the local Ethical Committee of the University of Pisa, in conformity with the Directive 2010/63/EU (project license n°39E1C.N.5Q7 released on 30/10/2021). C57BL/6 J mice were kept in a regulated environment (23±1 °C, 50 ± 5 % humidity) with a 12 h light-dark cycle with food and water *ad libitum*.

2.2. Cell cultures

Hippocampal neuron (HN) cultures were obtained from post-natal animals (P1 stage) as described in [21,23,26,27]. After isolation, cells were seeded in adhesion medium consisting of high-glucose Dulbecco's Modified Eagle's Medium (DMEM) (Gibco, Thermo Fisher Scientific, Waltham, Massachusetts, US, #21063-029) modified with 10 % fetal bovine serum (FBS) (Gibco; Thermo Fisher Scientific, Waltham, Massachusetts, US, #10270-106), 100 IU/ml penicillin, 100 μg/ml streptomycin (Gibco, Thermo Fisher Scientific, Waltham, Massachusetts, US, #15140-122) and 2 mM Glutamax (Gibco, Thermo Fisher Scientific, Waltham, Massachusetts, US, #35050-038) on 13 mm glasses pre-coated with 100 μg/ml poly-L-lysine (PLL, Merck, Sigma-Aldrich, Burlington, Massachusetts, US, #P4707), unless stated otherwise. The medium was replaced 4 h later with growth medium consisting of Neurobasal-A medium (Gibco, Thermo Fisher Scientific, Waltham, Massachusetts, US, #12,348–017), modified with 2 % (v/v) B27 (Gibco, Thermo Fisher Scientific, Waltham, Massachusetts, US, #17504-044), 2 mM Glutamax, 50 IU/ml penicillin, 50 μg/ml streptomycin.

Progenitors cells used in this work are SC derived human neuroepithelial stem (SC–NES) cells, gently donated by Prof. Marco Onorati and cultured as described by [28,29].

Murine J774 macrophage cells (American Type Culture Collection; ATCC, Manassas, USA) were tested for contamination and then grown in high-glucose DMEM (Gibco, Thermo Fisher Scientific, Waltham, Massachusetts, US, #31966-021), 1 % L-glutamine (Gibco, Thermo Fisher Scientific, Waltham, Massachusetts, US, #25030081), 1 % NEAA (non-essential amino acids) (EuroClone, Milan, IT, #ECB3054D), 10 % FBS (Gibco, Thermo Fisher Scientific, Waltham, Massachusetts, US, #A52567-01) and 1 % penicillin/streptomycin (Gibco, Thermo Fisher Scientific, Waltham, Massachusetts, US, #15070-063) at 37 °C in a 95 % O_2 and 5 % CO_2 humidified chamber. $6{\cdot}10^5$ cells were seeded in 100 mm cell culture dishes and, the day after, treated with 100 ng/ml lipopolysaccharide (LPS) (Merck, Sigma-Aldrich, Burlington, Massachusetts, US, #L4391, 0111:B4) for 5 h. The conditioned medium (CM) - unstimulated or LPS-stimulated - of J774 cells was collected and frozen at −80 °C.

2.3. Mouse organotypic spinal cord model: spinal cord slices

SC slices were generated as previously described [25,27,30]. Briefly, spinal cords were isolated from P3 mice, cut in 350 μm thick slices through a tissue chopper (McIlwain Tissue Chopper, Campden Instruments, Loughborough, UK), and kept on ice. Slices were cultured on Millicell membranes (Millipore, Merck, Burlington, Massachusetts, US, #PICM0RC50) coated with a solution containing 100 μg/ml collagen (Merck, Burlington, Massachusetts, US, #C7661), 100 μg/ml PLL and 10 μg/ml laminin (Merck, Sigma-Aldrich, Burlington, Massachusetts, US, #L2020) in minimal essential medium (Gibco, Thermo Fisher Scientific, Waltham, Massachusetts, US, #11090-081) with the addition of 25 % (v/v) Hank's Balanced Salt Solution (Gibco, Thermo Fisher Scientific, Waltham, Massachusetts, US, #14025-050), 25 % (v/v) horse serum (Gibco, Thermo Fisher Scientific, Waltham, Massachusetts, US, #16050-122), 25 mM HEPES buffer solution (Gibco, Thermo Fisher Scientific, Waltham, Massachusetts, US, #15630-056), 35 mM D-glucose (Merck, Sigma-Aldrich, Burlington, Massachusetts, US, #G7021), 2 mM Glutamax, 100 IU/ml penicillin, 100 μg/ml streptomycin and 100 ng/ml glial-derived neurotrophic factor (GDNF) (PeproTech, Thermo Fisher Scientific, Waltham, Massachusetts, US, #450-10). SC slices were placed in the Millicell membranes with the dorsal-ventral axis in the radial direction outward.

The medium was replaced at day *ex vivo* (DEV)0, and DEV1.. From DEV3 the medium was replaced with the organotypic medium (OM) consisting of Neurobasal medium modified with 2 % (v/v) B27, 1 % (v/v) N2 (Gibco, Thermo Fisher Scientific, Waltham, Massachusetts, US, #17502-048), 10 μg/ml insulin (Merck, Sigma-Aldrich, Burlington, Massachusetts, US, #I9278), 1 % (v/v) Glutamax, 1 % Pen/Strep, and 100 ng/ml GDNF. SC slices were maintained at 37 °C in a saturated humidity atmosphere of 95 % air and 5 % CO_2.

2.4. Drug treatment

HN cultures were exposed to compounds that inhibit axon growth. For CSPG treatment, glass coverslips have been coated with 100 μg/ml PLL for 4 h, and 0.5-1.5 μg/ml of CSPGs (Millipore, Merck, Burlington, Massachusetts, US, #CC117) for 90 min at 37 °C. For LPS treatment, LPS from E. coli (Merck, Sigma-Aldrich, Burlington, Massachusetts, US, #L4391, 0111:B4) was used. LPS was added to the medium at day *in vitro* (DIV)1 at the concentration of 5/10/20 ng/ml. For SEMA3A treatment, Recombinant Human Semaphorine 3A Fc Chimera Protein (Bio-Techne, R&D System, Minneapolis, Minnesota, US, #1250-S3) was used. SEMA3A was added to the medium at DIV1 at the concentration of 400 or 800 or 1600 ng/ml.

To induce a neuroinflammatory response in SC slices, LPS was added in the medium at a final concentration of 5 or 10 or 20 ng/ml at DEV3 and DEV5.

For cytokine treatment, the macrophage supernatant was added 1:10 in cell growth media at DIV0 for HNs and DEV3 for SC slices. This conditioned medium was supplemented with the cytokine cocktail: interleukin-1β (IL-1β) 50 U/ml (357pg/ml) (Bio-Techne, R&D System, Minneapolis, Minnesota, US, #201-LB-005), tumor necrosis factor α (TNFα) 1000 U/ml (3.7 ng/ml) (Merck, Sigma-Aldrich, Burlington,

Massachusetts, US, #T7539), interferon-γ (IFNγ) 1000 U/ml (5 ng/ml) (Roche, Basel, CH, #11040596001), and interferon-α (IFNα) 2000 U/ml (Bio-Techne, Minneapolis, Minnesota, US, #11100-1).

2.5. ELISA test

ELISA (enzyme-linked immunosorbent assay) tests against the pro-inflammatory cytokines TNFα and IL-6 (interleukin 6) were conducted for SC slices and macrophages cultured both in the presence or absence of LPS (5 or 10 or 20 ng/ml for SC slices, 100 ng/ml for macrophages). Two specific kits were used: Mouse TNFα Uncoated ELISA kit (Invitrogen, Thermo Fisher Scientific, Waltham, Massachusetts, US, #88-7324) for TNFα and Mouse IL-6 Uncoated ELISA kit (Invitrogen, Thermo Fisher Scientific, Waltham, Massachusetts, US, #88-7064) for IL-6. For SC slices, on every medium change the exhausted medium (1 ml) was collected and centrifuged at 1500 rpm for 5 min at 4 °C. Then, the pellet was discarded and the remaining supernatant stored at −80 °C until the time of use. For macrophages, the medium was collected after 5 h or 18 h (both from treated and untreated cultures) post-LPS treatment and stored at −80 °C until the time of use. ELISA tests were conducted according to the manufacturer's instructions. TNFα and IL-6 concentrations were expressed as picograms per milliliter (pg/ml). The lower assay limit of detection was 8 pg/ml for TNFα and 4 pg/ml for IL-6.

2.6. RNA extraction and quantification

Total RNA was extracted from control or LPS-treated (10 ng/ml) SC slices at DEV4 and from control or LPS-treated (10ng/ml) HN cultures at DIV3. For the RNA extraction NucleoSpin® RNA PLUS XS (Macherey-Naghel, Düren, Germany, #740990.50) was used. The procedure was conducted according to the manufacturer's instructions, on ice and in sterile conditions. The extracted RNA was quantified with the DeNovix DS-11 FX.

2.7. Real-time qPCR

The real-time qPCR was performed on RNA extracted at DEV4 from control or LPS-treated (10 ng/ml) SC slices and at DIV3 from control or LPS-treated (10 ng/ml) HN cultures. The procedure was conducted according to the manufacturer's instructions. Briefly, the RNA was converted into cDNA by using the iScriptTM Reverse Transcriptase from iScriptTM cDNA synthesis kit (Biorad, Hercules, California, US). For the real-time qPCR, SYBR green was used. The primers were the following: TNFα AssayID: qMmuCED0004141 (Biorad, Milan, IT); IL-6 AssayID: qMmuCID0005613 (Biorad, Milan, IT); IL-1β AssayID: qMmuCID0005641 (Biorad, Milan, IT). GAPDH (glyceraldehyde-3-phosphate dehydrogenase) (AssayID: qMmuCED0027497, Biorad, Milan, IT) was used as housekeeping.

2.8. Cell microinjection into the SC slices

SC–NES cells were transplanted into the SC slices using appropriate microneedles and a microinjector, as previously described [25,30]. SC–NES cells were loaded with MNPs at DIV7. The microinjection procedure was performed into DEV4 SC slices and after 10 days of SC–NES cell differentiation (DIV10). For microinjection, SC–NES cells were prepared as follows: after a wash with DPBS (Gibco, Thermo Fisher Scientific, Waltham, Massachusetts, US, #14190-144), they were detached with 0.25 % Trypsin-EDTA (Gibco, Thermo Fisher Scientific, Waltham, Massachusetts, US, #25200-056) and counted, stained with 1 μg/ml Dil red dye (Cell tracer TM Yellow stain, Thermo Fisher Scientific, Waltham, Massachusetts, US, #C34567), kept 20 min in an incubation bath at 37 °C, and resuspended in differentiation medium to reach a cell concentration of 3–5·10^4 cells/μl. Microneedles were then loaded with a volume of 4 μl of cell suspension using a micropipette, and, after calibration, 4 nl of cell suspension was microinjected into the ventral horns of DEV4 slices under a stereomicroscope.

2.9. Magnetic nanoparticles

MNPs used in this study are superparamagnetic iron oxide-based nanoparticles, Viscover^{TM} (XL FeraSpin, #130095173, MNP), characterized by a hydrodynamic diameter of 50–60 nm and capable of responding to the application of external magnetic fields. Viscover^{TM} products are developed and manufactured by nanoPET Pharma GmbH for preclinical studies (https://www.viscover-online.de/mri-portfolio/) [31,32]. MNPs have been added to the cell growth medium at the concentration of 100 μM of iron. Cell toxicity data are provided in Fig. S1. Both for HNs and SC slices, experiments were conducted in 35 mm Petri dishes placed inside a Halbach-like cylinder magnetic applicator, which provided a constant magnetic field gradient of 46.5 T/m in the radial centrifugal direction [22,33] (Fig. S2).

2.10. Magnetic nano-pulling

For HNs, the cell growth medium was modified with 5 µg/ml MNPs four hours after seeding. The magnetic field (stretch group) or a null magnetic field (control group) was applied from DIV1 for 48 h (short-term stimulation) or 120 h (long-term stimulation). For SC–NES cells, at DIV7 they were detached and reseeded in the differentiation medium and four hours later MNPs were added. In cell transplantation experiments, the magnetic field (stretch group) or a null magnetic field (control group) was applied from DEV5 (SC–NES cells were at DIV11) for 48 h.

2.11. Immunostaining and imaging

For HNs, after one wash with DPBS, cells were fixed in 2 % paraformaldehyde (PFA, Merck, Sigma-Aldrich, Burlington, Massachusetts, US, #P6148 500 G) and 7.5 % saccharose for 20 min and washed again three times with DPBS. Samples were permeabilized in 0.5 % Triton X-100 for 10 min at RT. Samples were then blocked in 5 % serum, 0.3 % Triton X-100 in DPBS for 1 h at RT. As primary antibody, βIII-tubulin (TUBBIII) (Merck, Sigma-Aldrich, Burlington, Massachusetts, US, #T8578, 1:500) was used, diluted in 3 % serum, 0.2 % Triton X-100 in DPBS. After overnight (ON) incubation at 4 °C, samples were washed and then incubated with the secondary antibody (Thermo Fisher Scientific, Waltham, Massachusetts, US, #A11029, 1:500) and Hoechst 33,342 (Thermo Fisher Scientific, Waltham, Massachusetts, US, #H3570, 1:1000) for 1 h at RT. Imaging was performed using a fluorescent microscope (TE2000-U, Nikon, Tokyo, Japan) equipped with DS-Ri2 camera with 10X objective. Images were acquired with a 2136 × 2136 pixel resolution and a 405 nm laser (425–475 emission filter) or a 488 nm laser (500- 550 emission filter). Images were acquired randomly along the edge of the glass on which the cells had been seeded.

Concerning SC slices, after two washes with DPBS they were fixed in 4 % PFA for 30 min at RT and washed again three times in DPBS. Samples were then permeabilized with 0.7 % Triton -X-100 in DPBS for 10 min at RT. Next, samples were blocked in 10 % serum, 0.5 % Triton X-100 in DPBS for 1 h at RT for 4 h at 4 °C. As primary antibody, cleaved caspase-3 (cCasp3) (Cell-Signaling, Danvers, Massachusetts, US, #9661, 1:500) or human Nestin (hNestin) (Bio-Techne, R&D systems, Minneapolis, Minnesota, US, #MAB1259, 1:400) were used, diluted in 1 % serum, 0.5 % Triton X-100 in DPBS. After ON incubation at 4 °C, samples were washed and then incubated with the secondary antibody (Thermo Fisher Scientific, Waltham, Massachusetts, US, #A11029 or Thermo Fisher Scientific, Waltham, Massachusetts, US, #A11011, 1:500) and Hoechst 33,342 (Thermo Fisher Scientific, Waltham, Massachusetts, US, #H3570, 1:1000) for 3 h at RT. For the immunostaining using ionized calcium-binding adapter molecule-1 (Iba1) antibody (Abcam, Cambridge, UK, #ab5076), after the washes in DPBS, samples were permeabilized with 0.4 % Triton X-100 in DPBS and blocked with 5 % horse serum. The primary antibody solution was then left incubating at 4 °C for 2 days. Next, secondary antibodies were normally

added. All samples were mounted on glass slides by using PolyMount solution (Aqua PolyMount, Polysciences, Warrington, Pennsylvania, US, #18606) and left drying ON prior to microscopy observation. Samples were imaged with a laser scanning confocal microscope (Nikon AX, Eclipse Ti2). Images were acquired with a 10 × objective or with a 20 × objective, a 1024 × 1024 pixel resolution and a 405 nm laser (420 nm - 476 nm emission filter) or a 488 nm laser (503 nm–541 nm emission filter) or a 561 nm laser (600 nm–625 nm emission filter).

2.12. Image analysis

Iba1-positive cells were counted in DEV7 SC slices that were positive to the marker Iba1 by using the software Fiji [34] with its plugin Analyze/Cell counter. Three regions of interest (ROI) per image from three different 20 × magnification images per SC slice (randomly acquired) were considered. Results were expressed as number of Iba1-positve cells per μm^2. For fluorescence quantification relative to the signal of Iba1, the mean fluorescence (background removed for each image) was performed using the software Fiji. Five regions of interest (ROI) per image from three different 20 × magnification images per SC slices (randomly acquired) were considered. The apoptotic rate was calculated as the ratio between cells positive both to Hoechst marker and cCasp3 marker on the total of Hoechst-positive cells. Apoptotic cells were counted by using the software Fiji with his plugin Analyze/Cell counter from three 20 × magnification images per SC slice. Images were acquired in Z-stack mode (series of ~20 optical plans per image with a step of 1 μm). For dose-response experiments and short-term stretching assay, the analyses of process length were performed by tracing single processes. The elongation was measured by using the plugin NeuronJ [35]. For HNs, 30 non-interconnected TUBBIII-stained neural neurites (the cut-off was fixed to 50 μm to distinguish axons from dendrites of DIV3 neurons) per replicate were analyzed from 10 × magnification images. For SC–NES cells microinjected into SC slices, 30 non-interconnected hNestin-stained neural processes per replicate were analyzed. The analysis was conducted on 10 × magnification images (randomly acquired) acquired in Z-stack mode (series of ~20 optical plans per image with a step of 2 μm). For long-term stretching assay on HNs, network analysis methods were chosen. The area of the neural process network was evaluated from five 10 × magnification images per replicate (randomly acquired). For each image, the network area was calculated as the ratio of the area occupied by neural processes and the area of the nuclei.

2.13. Statistical analysis

Data are reported as mean ± standard error of the mean (SEM) or data distribution (violin plot) from at least four replicates after blinded analyses (except for the stretching assay with inhibitory cocktail, which was performed on three replicates and the dose-response assay, which was performed on two replicates). Data were plotted with GraphPad software, version 9.5.1. The normality of the distribution was assayed by different tests, such as D'Agostino & Pearson normality test, KS normality test or Shapiro-Wilk normality test, and graphical representation. For normally distributed data, *t*-test for unpaired data followed by Bonferroni correction or two-way analysis of variance (ANOVA) test followed by Tukey's or Dunnett's multiple comparison were used. For non-normally distributed data, Mann-Whitney test was used. Significance was set at $p \leq 0.05$.

3. Results

3.1. Nano-pulling induces axon growth in hippocampal neurons cultivated in inhibitory conditions

CSPGs inhibit axon growth of developing neurons *in vitro* and *in vivo* [36]. Here, we cultured mouse HNs on CSPG-coated surfaces (Fig. 1A). First, we performed a dose-response assay to identify the CSPG concentration resulting in axon length reduction. Coating performed with CSPGs at the concentration of 1.5 μg/ml resulted in 31.5 % of reduction of axon length (from 149.8 ± 11.08 μm to 102.6 ± 6.20 μm, $p = 0.0013$) while the lower concentration (0.5 μg/ml) had no statistically significant effect compared to control neurons not cultured on CSPGs (from 149.8 ± 11.08 μm to 120.9 ± 9.46 μm, $p = 0.071$) (Fig. 1B). Based on these results, CSPGs at the concentration of 1.5 μg/ml was used in the following experiments. First of all, HNs were subjected to nano-pulling for 48 h in presence or absence of CSPG-coating (not stretched cells were used as a control), and analysis of axon length was performed at DIV3 (Fig. 1A and C, short-term assay, ts=48 h). Single axon tracing was performed with NeuronJ (Fig. 1C, no treatment and CSPG treatment ts=48 h). As expected, the CSPG coating induced a reduction of the axon length, however, the nano-pulling counteracted the CSPG-induced axon shortening, as documented by the stretched condition that reached control levels (the axon length of neurons cultured on CSPGs and in the absence of CSPGs was 146.7 ± 5.3 μm and 131.8 ± 3.6 μm, respectively, $p = 0.11$) (Fig. 1D). Then, we prolonged the stimulation up to 120 h (Fig. 1A and C, long-term assay, ts=120 h), when neurons show a strong arborization of their processes, and the network can be analysed as the area covered by the neuronal processes normalized to the area covered by the nuclei. As expected, the CSPG treatment reduced the neurite network (Ctrl/CSPG$^-$ vs Ctrl/CSPG+ was 5.07±0.22 and 4.23±0.17, respectively, $p = 0.021$). With the prolonged mechanical stimulation, the boosting effect of the nano-pulling was even more evident. In fact, the stretched CSPG-treated group showed a 10 % increase with respect to the CSPG-untreated control group that does not reach statistical significance (CSPG-/Ctrl vs CSPG+/Stretch is 5.07±0.22 and 5.56±0.21, respectively, $p = 0.32$) (Fig. 1E).

Inhibition from the component of the extracellular matrix is not the only mechanism impairing axon growth. A crucial role is also played by inflammation typically occurring in neurodegenerative disorders. We validated the ability of nano-pulling to induce stretch-growth in an inflammatory condition induced by LPS, an immunogen agent [37] (Fig. 2A1). Since our mouse primary cultures are hippocampal neurons growing onto a layer of glial cells (Fig. 2A2), we hypothesized that the incubation with LPS can trigger over-expression of inflammatory cytokines. LPS was used at 10 ng/ml, as suggested by the existing literature [38]. The expression levels of the pro-inflammatory cytokines TNFα, IL-6, and IL-1β was evaluated by analysing mRNA. We found that LPS induces a strong increase in IL-1β (5.81±1.93 fold change with respect to the control, $p = 0.047$, Fig. 2B1) and in IL-6 (7.04±0.76 fold change with respect to the control, $p = 0.0002$, Fig. 2B2) and a moderate increase in TNFα (14 % increase, $p = 0.048$ Fig. 2B3). Having confirmed the overexpression of pro-inflammatory cytokines, we tested nano-pulling in LPS-treated cultures (Fig. 2C1). As expected, LPS treatment was found to reduce axon length (Ctrl/LPS- vs Ctrl/LPS+ was 147.94±4.99 μm vs 123.60±4.71 μm, $p = 0.016$) (Fig. 2C2). Nano-pulling resulted not only in a restoration effect but also in the enhancement of the axon length of LPS-treated stretched axons compared to the LPS-untreated control axons (Stretch/LPS+ vs Ctrl/LPS- was 189.03±6.66 μm vs 147.94±4.99 μm, $p < 0.0001$) (Fig. 2C2). Interestingly, nano-pulling appeared to induce axon growth at the same rate independently of the presence of the inflammatory agent (Stretch/LPS- vs Stretch/LPS+ was 205.77±6.49 μm vs 189.03±6.66 μm, $p = 0.17$).

However, following a CNS injury, neuroinflammation results from a highly complex response involving both resident microglia and infiltrating macrophages that are recruited to the site of damage. These immune cells release a broad spectrum of pro-inflammatory cytokines that amplify immune and inflammatory cascades [39]. To model this intricate response *in vitro*, we cultured HNs with conditioned medium (CM) derived from J774 mouse macrophages, either unstimulated or stimulated with LPS (Fig. 3A). First, we assessed the presence of key inflammatory cytokines—IL-6 and TNF-α—in the macrophage CM using ELISA. We found negligible (below detection limit) cytokine lev-

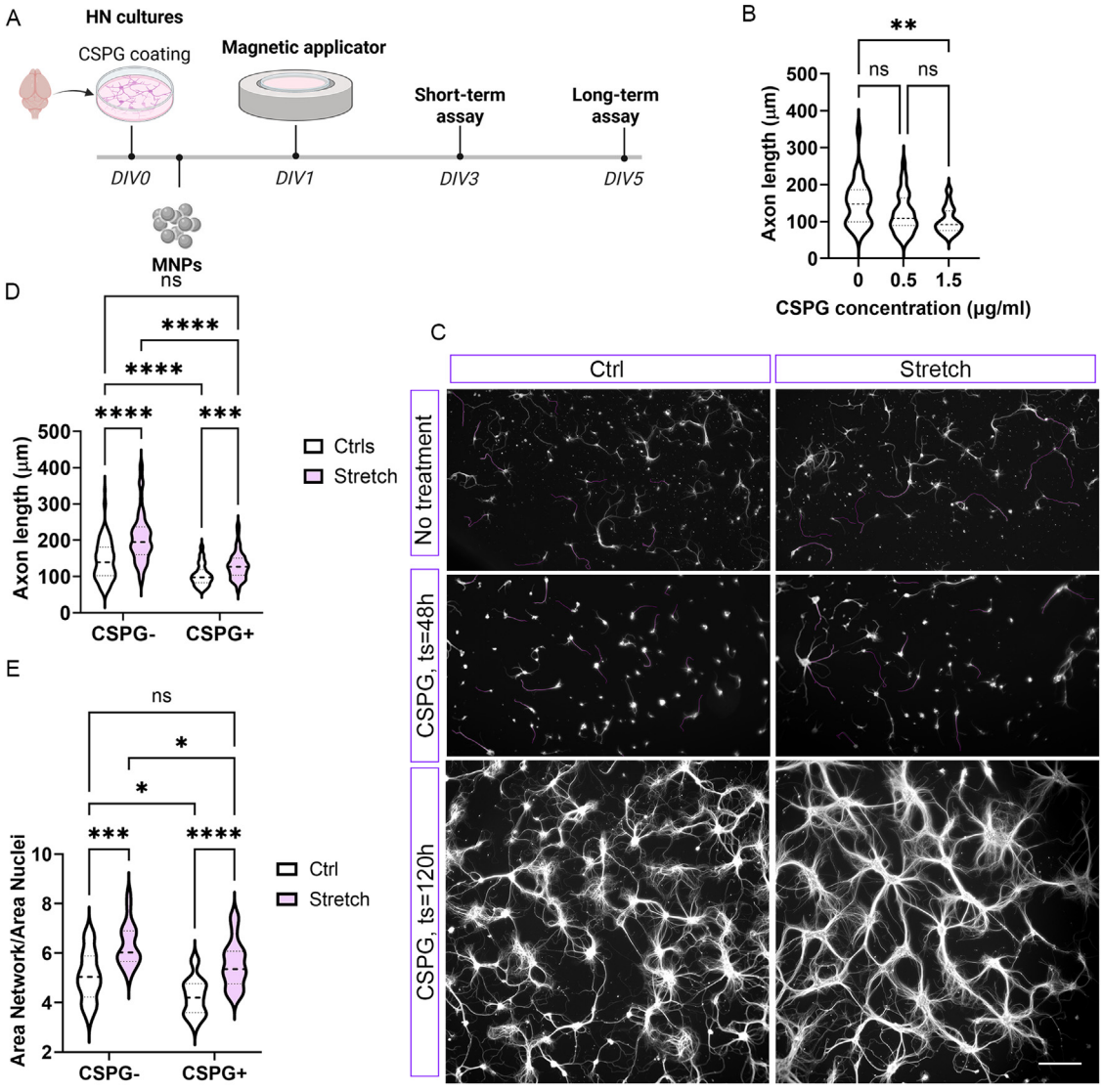

Fig. 1. Effect of CSPG coating on axon length of primary mouse HNs. (A) Timeline of the experiment: MNPs 5 µg/ml are added to cell growth medium 4 h after cell seeding (DIV0), the mechanical stimulation is performed at DIV1, analysis of axon length is performed at DIV3 for the short-term assay and DIV5 for the long-term assay. (B) Dose-response assay to CSPGs. Violin plot. $n = 60$ axons, from two replicates. One-way ANOVA, F = 6.777, $p = 0.0018$. (C) Representative images of HNs cultured on PLL-coated surfaces or PLL/CSPG-coated surfaces, in control or stretched conditions (TUBBIII staining). Magenta lines show examples of axon tracing. Scale bar: 200 μm. (D) Short term assay (stretching time ts=48 h). Axon length distribution. Violin plot. $n = 120$ axon, from four replicates. 2-way ANOVA followed by Tukey's multiple comparisons test. Interaction: F(1, 468)=15.89, $p < 0.0001$; row (CSPG): F(1, 468)=165, $p < 0.0001$; columns (stretch): F(1, 468)=94.04, $p < 0.0001$. (E) Long-term assay (stretching time ts=120 h). Analysis of the neurite network. The surface area of the network is normalised to the surface area of the nuclei in the same ROI. Violin plot. $n = 20$ images, from four replicates. 2-way ANOVA followed by Tukey's multiple comparisons test. Interaction: F(1, 76)=0.02696, $p = 0.87$. Row (CSPG): F(1, 76)=16.23, $p = 0.0001$. Columns (stretch): F(1, 76)=41.90, $p < 0.0001$.

els in CM from unstimulated macrophages (Fig. 3B). In contrast, LPS-stimulated macrophages produced high cytokine levels at both 5 and 18 h post-treatment, with IL-6 reaching approximately 200 pg/ml and TNF-α around 70 pg/ml (Fig. 3B).

The macrophage CM was diluted 1:10 (v/v) in growth medium (GM). To further enhance the neuroinflammatory environment, the GM/CM was supplemented with a cytokine cocktail (Fig. 3A). This cocktail included: IL-1β, a pleiotropic cytokine predominantly produced by activated microglia and astrocytes [40]; TNF-α, a mediator of the neuroinflammation associated with neurodegeneration [41]; IFN-γ, commonly upregulated in neurodegenerative and neuroinflammatory diseases and known to cause neuronal damage under chronic inflammatory conditions [42]; and IFN-α, which has been shown to impair endogenous neurogenesis, axon growth, neuronal survival, and neurotrophic signaling in the hippocampus [43]. Hereafter, this medium is referred to as cytokine cocktail medium (CK-M), while CTRL-M indicates GM supplemented with 1:10 dilution of CM derived from unstimulated macrophages and not supplented with cytokines. Neurons cultured in CTRL-M exhibited an average axon length of 134.01 ± 5.26 µm, which was shorter than that of neurons cultured in GM (147.94 ± 4.99 µm, Fig. 2C2). An additional 19 % reduction in axon length was observed in neurons cultured in CK-M (109 ± 4.10 µm, Fig. 3C). Interestingly, nano-pulling induced a 31 % increase in axon length in neurons cultured in CK-M (from 109 ± 4.10 µm in control neurons to 142.97 ± 4.81 µm in stretched neurons, $p < 0.001$; Fig. 3C), resulting in a full recovery of axon length to a level comparable with that of neurons cultured in GM (147.94 ± 4.99 µm, Fig. 2C2). Representative fluorescence images corresponding to these experimental conditions are shown in

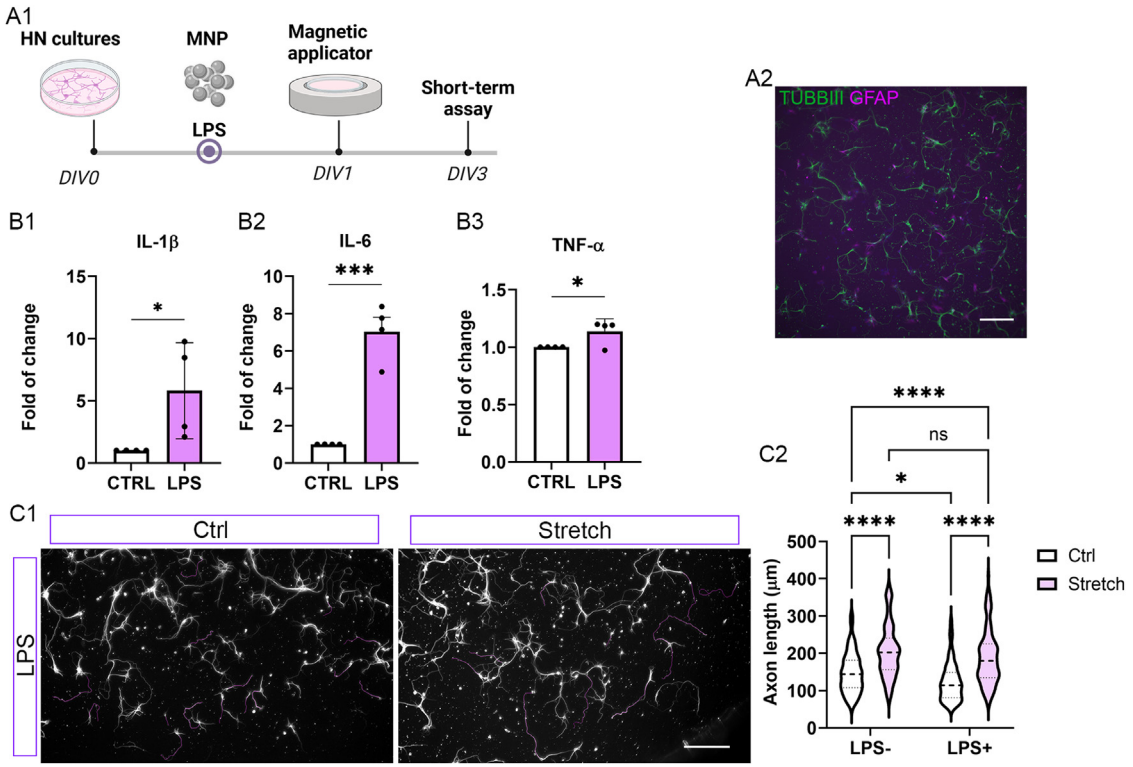

Fig. 2. Response to LPS-induced inflammation. (A1) Timeline of the experiment: 4 h after cell seeding (DIV0), MNPs 5 μg/ml and LPS 10 ng/ml are added to cell growth medium; the mechanical stimulation is performed from DIV1 to DIV3. (A2) Mouse primary cultures contain a mixed population of neurons (TUBBIII-positive) and glial cells (GFAP-positive). Scale bar: 200 μm. (B) Real-time qPCR at DIV3 for the pro-inflammatory cytokines IL-1β (B1), IL-6 (B2), and TNFα (B3) performed in control or 10 ng/ml LPS-treated HNs. Unpaired t-test 2-tailed, $n = 4$. B1) $p = 0.047$, $t = 2.492$, df=6. (B2) $p = 0.0002$, $t = 7.897$, df=6. (B3) $p = 0.0476$, $t = 2.484$, df=6. (C1) Representative images of HNs treated with LPS in control or stretched conditions (TUBBIII staining). Magenta lines show examples of axon tracing. Scale bar: 200 μm. Untreated cultures shown in Fig. 1C. (C2) Distribution of axon length. Violin plot. $n = 120$ axons, from four replicates. 2-way ANOVA followed by Tukey's multiple comparisons test. Interaction: F(1, 470)=0.4317, $p = 0.5115$. Row (LPS): F(1, 470)=12.65, $p = 0.0004$. Column (stretch): F(1, 470)=113.8, $p < 0.0001$.

Fig. 3D, highlighting the differences in axonal morphology among the treatments.

As subsequent step, we tested the nano-pulling in the presence of SEMA3A, a neurotrophin that reduces sprouting and axon length in HNs [44]. First, we performed a dose-response assay to find the dose of SEMA3A able to reduce axon length (Fig. 4A1). 800 ng/ml SEMA3A resulted in 22 % of neurites length reduction (from 144.9 ± 5.82 μm to 119.0 ± 6.07 μm, $p = 0.009$) so it was chosen for the model set up, while the lower concentration (400 ng/ml) had no statistically significant effect compared to control neurons (Ctrl vs SEMA3A 400 ng/ml was 144.9 ± 5.82 μm and 149.6 ± 6.59, respectively, $p = 0.94$). The effect of the higher concentration (1.6 μg/ml) is not statistically different compared to 800 ng/ml ($p = 0.95$), thus indicating a saturation effect (Fig. 4A1). Mechanical stimulation displayed a restoration effect also in the SEMA3A inhibitory model (Fig. 4A2), bringing SEMA3A treated and stretched axons similarly in length to untreated control axons (Ctrl/SEMA3A- vs Stretch/SEMA3A+ was 153.5 ± 5.5 μm vs 165.9 ± 5.1 μm, respectively, $p = 0.42$) (Fig. 4A3).

Finally, we exposed the HNs to a cocktail of inhibitory signals, involving the simultaneous administration of CSPGs, LPS, and SEMA3A (Fig. 4B1). While individual treatments generally led to a 20 % reduction in axon length, the decrease was more pronounced with the cocktail (35 %, yielding a length of 147.9 ± 5.06 μm and 95.90±2.61 μm in control cultures without and with the CSPGs/LPS/SEMA3A treatment, respectively; $p < 0.0001$, Fig. 4B2, B3). Despite the strong inhibition of spontaneous elongation, nano-pulling was able to induce a 25 % increase in axon length in cultures treated with CSPGs/LPS/SEMA3A (95.90±2.61 μm and 119.9 ± 3.25 μm for control and stretched cultures, respectively; $p = 0.0013$, Fig. 4B3).

3.2. *Generation of an* ex vivo *model to test nano-pulling in the presence of inflammation in the spinal cord tissue*

In this study, we developed an organotypic model that accounts for inflammation state that occurs in the spinal cord tissue during injuries [15,45,46]. This model will be used subsequently to test the effects of nano-pulling on transplanted progenitor cells. Progenitor cells used in this work are spinal cord derived human neuroepithelial stem cells [28,29].

Spinal cord slices represent a transection model but typically stabilize after a few days in culture [30]. We aimed to determine whether spinal tissue sectioning alone is sufficient to trigger a sustained inflammatory condition. A similar evaluation was carried out on SC slices pre-treated with LPS, a widely recognized immunogen capable of stimulating an inflammatory response in organotypic models [47,38].

The presence of inflammation was evaluated by analysing mRNA or protein expression levels of the pro-inflammatory cytokines TNFα, IL-6, and IL-1β, [48] as they are primary initiators and effectors of the inflammatory cascade typical of acute, and particularly secondary spinal cord injury (SCI).

Tests were performed on the culture media collected during media changes (i.e., DEV0, DEV1, DEV3, DEV5, DEV7) from SC slices in culture. DEV0, DEV1, and DEV3 represent the initial time points in culture, allowing us to evaluate the direct effect of tissue sectioning on inflammation induction. Measurements at DEV5 and DEV7 are the specific time points to assess the presence of inflammation after the tissue had stabilized and following the transplantation of SC–NES cells, respectively (Fig. 5A).

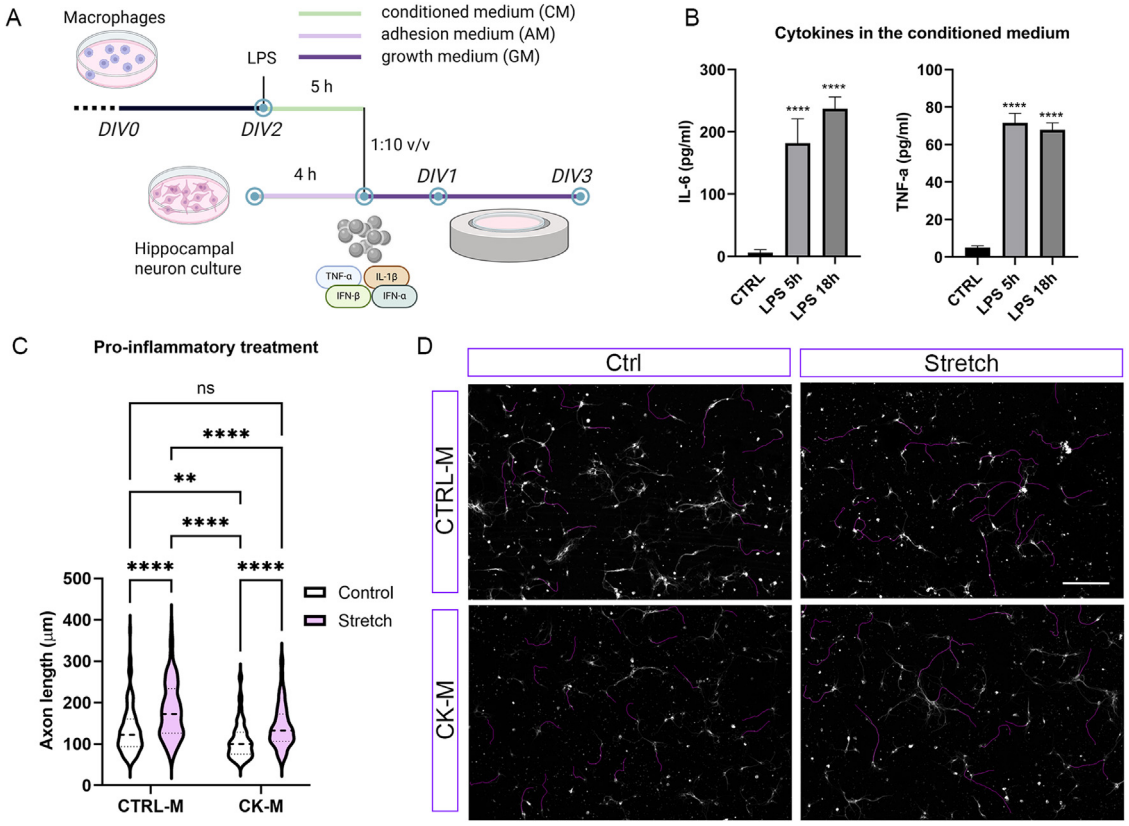

Fig. 3. Response to cytokine-induced inflammation. (A) Timeline of the experiment: 4 h after cell seeding (DIV0), GM is modified with MNPs 5 μg/ml, LPS-treated macrophage CM (CM:GM was 1:10), and IL-1β 50 U/ml, TNFα 1000 U/ml, IFNγ 1000 U/ml, and IFNα 2000 U/ml. In the control group (CTRL-M), the GM is modified with MNPs 5 μg/ml and macrophage CM (no treatment with LPS) 1:10. The mechanical stimulation is performed from DIV1 to DIV3. (B) ELISA tests for the quantification of the pro-inflammatory cytokines IL-6 and TNFα in the CM collected from macrophages not treated with LPS (CTRL) or after 5 or 18 h of treatment with LPS. One-way ANOVA followed by Tukey's multiple comparison test, $n = 4$. For IL-6: F (2, 8)=68.16, $p < 0.0001$. Kit detection limit: 4 pg/ml. For TNFα: F (2, 9)=409.7, $p < 0.0001$. Kit detection limit: 8 pg/ml. (C) Distribution of axon length. Violin plot. $n = 120$ axons, from four replicates. 2-way ANOVA followed by Šídák's multiple comparisons test. Interaction: F (1, 476)=1.590, $p = 0.21$. Row (treatment): F (1, 476)=37.30, $p < 0.0001$. Column (stretch): F (1, 476)=61.47, $p < 0.0001$. (D) Representative images of HNs (TUBBIII staining). Magenta lines show examples of axon tracing. Scale bar: 200 μm.

The ELISA tests for TNFα and IL-6 cytokines revealed that SC tissue sectioning alone is insufficient to produce a significant or persistent inflammatory state in SC slices. The concentrations of TNFα and IL-6 were very low at all time points, becoming negligible after DEV3, when SC slices stabilized (Fig. 5B1/2). Specifically, for both cytokines, an initial increase in production was observed (DEV0 for TNFα, DEV1 for IL-6, Fig. 5B1/2), but levels rapidly decreased at subsequent time points, returning to baseline.

Given that untreated SC slices did not exhibit a significant or sustained inflammatory state, we repeated the evaluation on SC slices pretreated with LPS. To induce a prolonged inflammatory state, LPS was administered at two successive time points, DEV3 and DEV5 (Fig. 5A), which correspond to the periods immediately before and after the planned cell microinjection at DEV4. LPS treatment led to an increase in cytokine levels. For TNFα, the increase was statistically significant compared to the control (0 pg/ml) at the LPS concentration of 10 ng/ml (46.78±12.60 pg/ml, $p < 0.001$) and 20 ng/ml (75.30±20.22 pg/ml, $p < 0.001$), but not at 5 ng/ml (14.86±4.11 pg/ml, $p = 0.26$). For IL-6, the increase was significant at 10 ng/ml (89.20±22.82 pg/ml, $p = 0.075$) and 20 ng/ml (243.49±65.40 pg/ml, $p < 0.001$), but not at 5 ng/ml (30.96±18.52 pg/ml, $p = 0.56$). At DEV7, a statistically significant increase was observed at all tested concentrations for TNFα, and at 10 and 20 ng/ml (but not 5 ng/ml) for IL-6. These results demonstrated that the minimum LPS concentration required to induce a significant cytokine increase compared to the control was 10 ng/ml. Therefore, LPS was used at 10 ng/ml for subsequent experiments.

To confirm the ELISA results and further investigate the inflammatory status at the time point designated for SC–NES cell transplantation (DEV4), we performed real-time qPCR on RNA extracted from control and LPS-treated SC slices at DEV4. The data showed that LPS treatment increased expression of IL-1β (8.56±1.29 fold change, $p = 0.0001$, Fig. 5D1), IL-6 (11.76±1.33 fold change, $p < 0.0001$, Fig. 5D2), and TNFα (1.90±0.24 fold change, $p = 0.0032$, Fig. 5D3), confirming the efficacy of LPS in inducing inflammation in this *ex vivo* model.

Inflammation was further validated using immunofluorescence to assess the activation of microglial cells, the primary drivers of immune responses in the CNS [49]. We used Iba1, a cytoplasmic protein expressed by immune-responsive cells like microglia, as a marker of activation (Fig. 5C1), since it is known to be overexpressed during microglial inflammatory activation [50]. At DEV7, we observed an increase in Iba1 mean fluorescence intensity (2.58±0.46 fold change, $p = 0.0042$, Fig. 5E1) and in Iba1-positive cells per μm^2 (4.37±0.72, $p < 0.0001$, Fig. 5E2), confirming the persistence of inflammation until the experiment conclusion. These findings, consistent with the ELISA and qPCR data, confirm that LPS at 10 ng/ml can induce a robust inflammatory state in this *ex vivo* model.

Finally, to ensure that LPS-induced inflammation did not compromise cell viability, SC slices were stained for the active form cCASP3 and compared to untreated slices. cCASP3 positivity appeared as small spots co-localizing with the nuclear marker Hoechst (Fig. 5C2). The apoptotic rate, defined as the percentage of cCASP3-positive cells relative to total cell count, was very low in both control slices (0.92±0.39 %) and LPS-

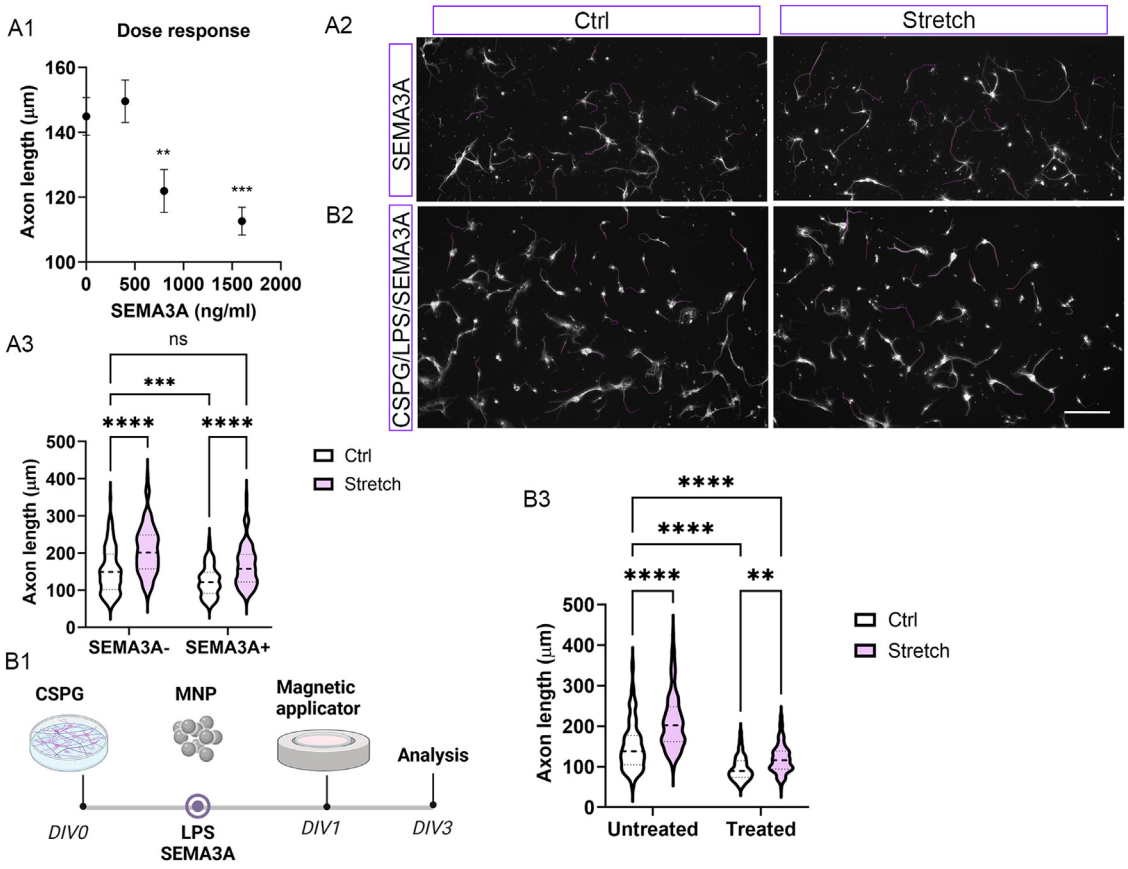

Fig. 4. Response to SEMA3A and inhibitory cocktail. (A1) Dose-response assay for SEMA3A. Violin plot. $n = 60$ axons, from two replicates. One-way Kruskal-Wallis's test. $p < 0.0001$. (A2) Representative images of HNs treated with SEMA3A in control or stretched conditions (TUBBIII staining). Magenta lines show examples of axon tracing. Untreated cultures shown in Fig. 1C. Scale bar: 200 μm. (A3) HNs are treated with SEMA3A 800 ng/ml. Violin plot. 2-way ANOVA followed by Tukey's multiple comparisons test. Interaction: F(1, 470)=1.815, $p = 0.18$. Row (SEM3A): F(1, 470)=48.05, $p < 0.0001$. Column (stretch): F(1, 470)=87.50, $p < 0.0001$. (B1) Timeline of the experiment with the inhibitory cocktail: cells are seeded on CSPG coating. 4 h after cell seeding (DIV0), MNPs 5 μg/ml, LPS 10 ng/ml and SEMA3A 800 ng/ml are added to cell growth medium; the mechanical stimulation is performed from DIV1 to DIV3. (B2) Representative images of HNs treated with CSPGs, LPS, SEMA3A in control or stretched conditions (TUBBIII staining). Magenta lines show examples of axon tracing. Untreated cultures are shown in Fig. 1C. Scale bar: 200 μm. (B3) Violin plot. $n = 120$ axon, from three replicates. 2-way ANOVA followed by Tukey's multiple comparisons test. Interaction: F(1, 483)=15.16, $p = 0.0001$. Row (treatment): F(1, 483)=253.9, $p < 0.0001$. Column (stretch): F(1, 483)=82.90, $p < 0.0001$.

treated slices (1.03±0.34 %), with no significant difference between the two conditions ($p = 0.60$, Fig. 5E3). The absence of a significant difference in apoptosis between conditions ruled out cell mortality as a potential confounder, leading us to conclude that LPS-induced inflammation is the sole factor affecting the experimental outcomes.

2.3. Nano-pulling stimulates the elongation of projections from neural progenitors transplanted into the organotypic model

The ability to induce guided growth of neural processes in neural progenitors transplanted into SC slices through nano-pulling was demonstrated in a previous study [25]. However, those data were collected from stabilized cultures that do not account for the inflammation characteristic of neurodegenerative processes. In this study, we aimed to determine whether inflammation could hinder force-mediated axon growth. To investigate this, we generated an organotypic model of spinal cord characterized by the presence of an inflammatory state (Fig. 5) and we transplanted neural progenitors into this model.

First, MNP-loaded human SC–NES cells were transplanted into control and LPS-treated mouse SC slices (Fig. 6A). The length of the processes of transplanted cells was assessed using human-specific antibodies for staining and traced using NeuronJ (Fig. 6C). Consistent with previous literature [51], LPS treatment resulted in a 20 % reduction in process length (control, LPS- vs. LPS+: 121.5 ± 5.07 μm vs. 98.08±3.41 μm, $p = 0.003$, Fig. 6B).

Mechanical stimulation alone significantly promoted elongation, inducing a 27 % increase in length (LPS-, control vs. stretched: 121.5 ± 5.07 μm vs. 154.2 ± 4.82 μm, $p < 0.0001$), in line with previous findings [25]. Interestingly, in the presence of LPS, the elongation rate following mechanical stimulation was remarkable, showing a 63 % increase (LPS+: control vs. stretched was 98.08±3.41 μm vs. 160.4 ± 4.67 μm, $p < 0.0001$). This suggests that under mechanical stimulation, LPS loses its inhibitory effect entirely, as indicated by the similarity in the lengths of the two stretched groups, with or without LPS (stretched: LPS- vs. LPS+ was 154.2 ± 4.82 μm vs. 160.4 ± 4.67 μm, $p = 0.7$).

Secondly, MNP-loaded human SC–NES cells were transplanted into mouse SC slices incubated in organotypic growth (OG) medium enriched with cytokines (CK-OG). Analogously to the experiments performed on HNs (Fig. 3), the CK-OG medium was prepared by diluting CM derived from LPS-stimulated macrophages 1:10 (v/v) in OG medium, and further supplemented with a cytokine cocktail consisting of IL-1β, TNF-α, IFN-γ, and IFN-α (Fig. 7A).

As expected, incubation in CK-OG resulted in a statistically significant reduction in the length of neural projections from SC–NES cells in the control group (125.44 ± 4.58 μm in OG medium vs. 94.43 ± 3.24 μm

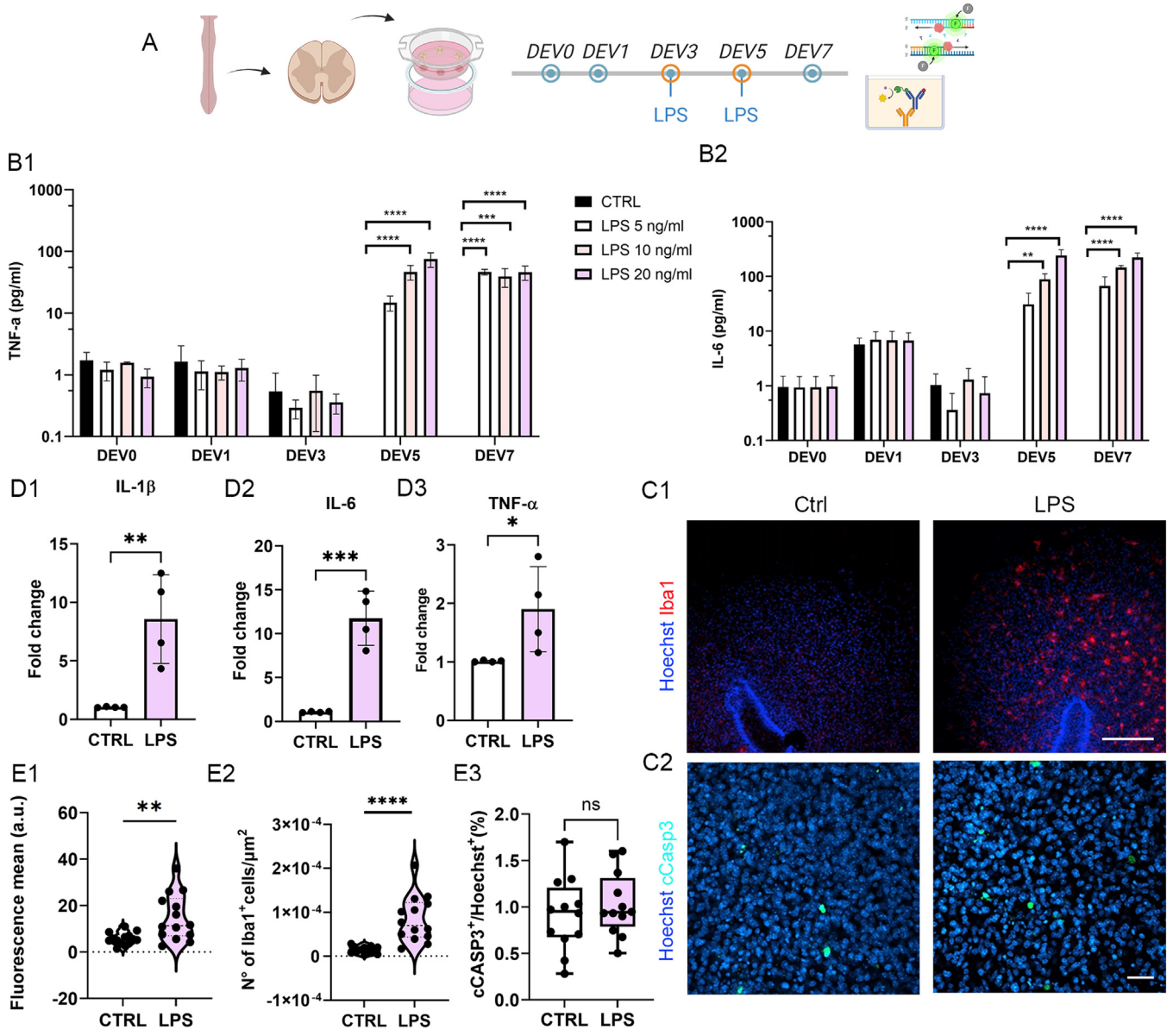

Fig. 5. Evaluation of the inflammatory status of SC slices after transection (DEV0) and *ex vivo* culturing (DEV0-7). (A) Timeline of the experiment. The addition of LPS is performed at DEV3 and DEV5. (B1) ELISA tests for the quantification of the pro-inflammatory cytokine TNFα. Two-way ANOVA followed by Dunnett's multiple comparison test. Interaction: F(12, 58)=6.335, $p < 0.0001$. Row (time): F(4, 58)=28.42, $p < 0.0001$. Column (LPS concentration): F(3, 58)=11.88, $p < 0.0001$. Kit detection limit: 8 pg/ml. B2) ELISA tests for the quantification of the pro-inflammatory cytokine IL-6 on the collected culture medium. For both graphs, the mean ± standard deviation is reported, $n = 4$ medium collections per time-point, bar graphs. Two-way ANOVA followed by Dunnett's multiple comparison test. Interaction: F(12, 58)=7.871, $p < 0.0001$. Row (time): F 4, 58)=26.88, $p < 0.0001$. Column (LPS concentration): F(3, 58)=20.16, $p < 0.0001$. Kit detection limit: 4 pg/ml. (C) Representative images of DEV7 SC slices in control or 10 ng/ml LPS-treated conditions. (C1) Hoechst/Iba1 staining. (C2) Hoechst/cCasp3 staining. Scale bar: 200 μm. (D) Real-time qPCR at DEV4 for the pro-inflammatory cytokines IL-1β (D1), IL-6 (D2), and TNFα (D3) performed in control or 10 ng/ml LPS-treated SC slices. For all graphs, the mean ± standard deviation is reported, *t*-test 2-tailed, $n = 4$ replicates. (D1) $p = 0.0073$, $t = 3.982$, df=6. (D2) $p = 0.0004$, $t = 6.945$, df=6. (D3) $p = 0.0497$, $t = 2.452$, df=6. (E1) Quantification of mean fluorescence of Iba1 in control and LPS-treated SC slices. Violin plot, Mann-Whitney test, $p = 0.0042$. (E2) Density of Iba1-positive cells in control and LPS-treated SC slices. Violin plot, Mann-Whitney test, $p < 0.0001$. (E1/2) $n = 14$ slices per condition. (E3) Comparison of the apoptotic rate in control and LPS-treated SC slices. Box plot, Mann-Whitney test, $p = 0.60$. $n = 12$ SC slices per condition.

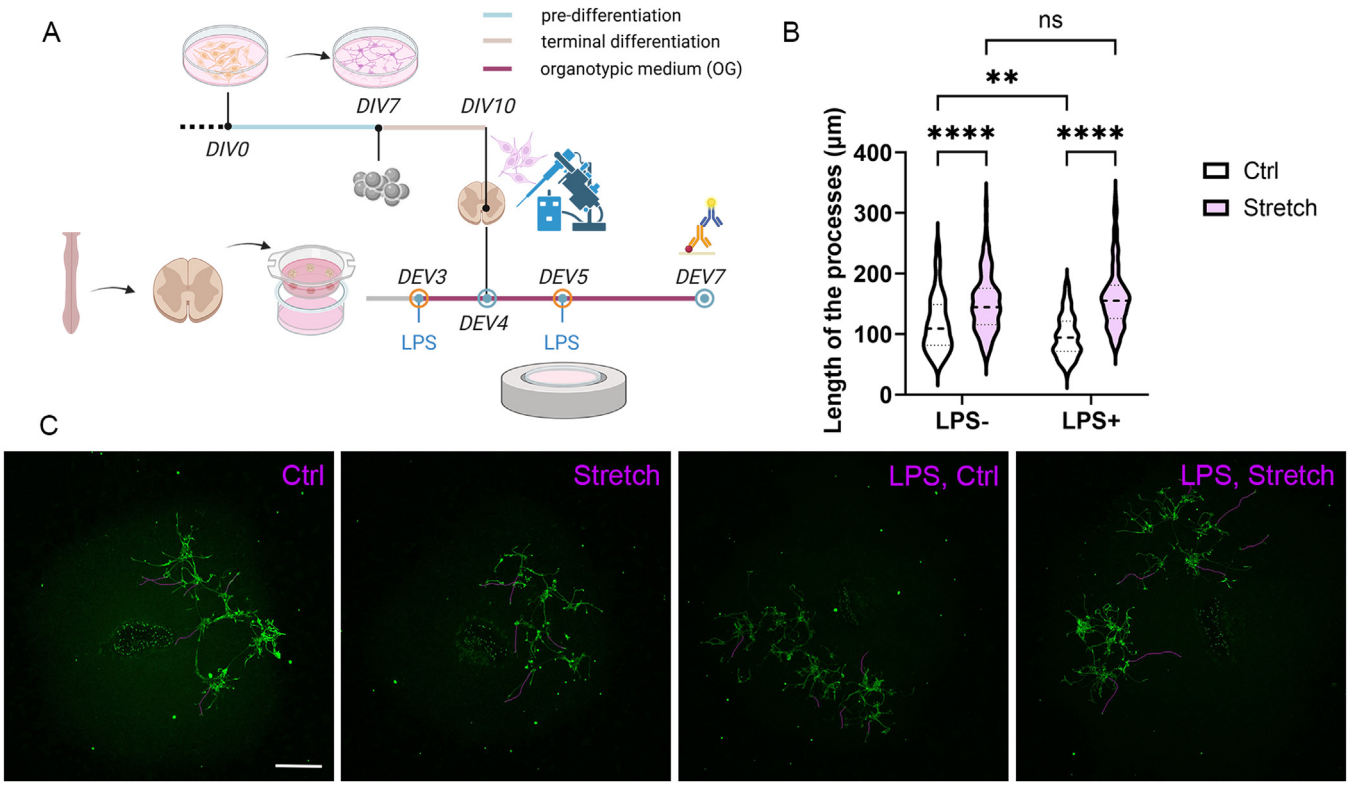

Fig. 6. Elongation of neural processes in SC–NES cells microinjected into control and LPS-treated SC slices. (A) Timeline of the experiment: neuronal progenitors are pre-differentiated, labelled with MNPs at the beginning of terminal differentiation (DIV7), and microinjected at DIV10 in DEV4 SC slices. SC slices are treated with LPS at DEV3 and DEV5. (B) Violin plot of axon length. Two-way ANOVA followed by Tukey's multiple comparison test. Interaction: $F(1, 472)=11.63$, $p = 0.0007$. Row (LPS): $F(1, 472)=2.320$, $p = 0.1284$, Column (stretch): $F(1, 472)=135.3$, $p < 0.0001$. $n = 120$ neuronal processes per group. (C) Representative images at DEV7 of cells transplanted in the SC slices, in control or stretched conditions, with and without LPS (human Nestin-staining). Scale bar: 250 µm.

in CK-OG medium, corresponding to a 25 % decrease, $p < 0.0001$; Fig. 7B).

However, when SC slices incubated in CK-OG were subjected to nano-pulling, the neural projections of SC–NES cells exhibited sustained growth (141.30 ± 4.43 µm), exceeding that of control SC–NES cells transplanted into SC slices cultured in OG medium (125.44 ± 4.58 µm, $p = 0.028$). This increase was comparable to that observed in stretched SC–NES cells transplanted into SC slices cultured in OG medium (145.01 ± 3.70 µm, $p = 0.91$). Representative fluorescence images of SC–NES cell projections under the different conditions are shown in Fig. 7C, illustrating the effects of cytokine exposure and nano-pulling on process outgrowth.

This statistical analysis highlights that mechanical stimulation can promote the elongation of neuronal processes in SC tissue even in the presence of inflammatory environment.

4. Conclusions

During the development of the CNS, axonal movement is influenced *in vivo* by chemo-attractive cues, which guide axons toward appropriate destinations, and chemorepellent signals, which discourage axon growth toward certain regions [52]. The best-characterized family of chemorepellent molecules is the semaphorins (from the Greek word "semaphore"). These molecules can bind to cell surfaces or the extracellular matrix, causing nearby axons to retract [12]. Additionally, certain components of the extracellular matrix (e.g., laminins, proteoglycans, fibronectin, tenascin) are finely regulated during development to control axon growth and pathfinding [53]. Following CNS injury, these inhibitory components are upregulated, posing a significant barrier to axon regeneration [2].

Beyond chemotaxis, axon navigation requires movement, and movement requires force. The growth cone generates a contractile force that pulls the axon shaft (F_{ax}) [54], who produces a contractile force that pulls the growth cone (F_{GC}) [55]. The balance between these two forces determines whether the axon tip protrudes ($F_{GC}>F_{ax}$) or retracts ($F_{GC}<F_{ax}$) [56]. By perturbating this balance, it is possible to modulate axon growth. In order to change force balance, in 2014, my research team introduced a novel technology called "nano-pulling," which uses magnetic nanoparticles to stretch axons by applying external magnetic fields. In mature neurons, nano-pulling enhances axon outgrowth and synaptic transmission [23], while in neural progenitors, it accelerates their differentiation into mature neurons and promotes the elongation of their processes [25]. Our previous mechanistic studies suggest that nano-pulling stabilizes microtubules (MTs) in both mature and immature neurons [21,25]. In fact, Nocodazole, which destabilizes MTs, but not Paclitaxel, which stabilizes them, has been shown to inhibit axon growth induced by nano-pulling, emphasizing the crucial role of MT stabilization [23]. Conversely, no effects have been detected following treatment with drugs that interfere with the actin cytoskeleton [23]. Nano-pulling is also inhibited when α-tubulin or β-tubulin is knocked out in the touch receptor neurons of *C. elegans* because this causes the formation of less stable microtubules (11-protofilament form). MT stabilization leads to an increase in axonal MT density [23,24]. It is still unclear how nano-pulling induces MT stabilization. MTs may be intrinsically mechanosensitive, or force may act through microtubule-associated proteins (MAPs), for example, by altering MAP activity or the interaction time between MTs and MAPs [57]. From a biophysical perspective, the pulling force generated by MT sliding and polymerization can reduce the axonal contractile force (F_{ax}), promoting tip advancement ($F_{GC}>F_{ax}$) [20]. At the functional level, considering that MTs provide the primary cytoskeletal tracks for axonal transport, their

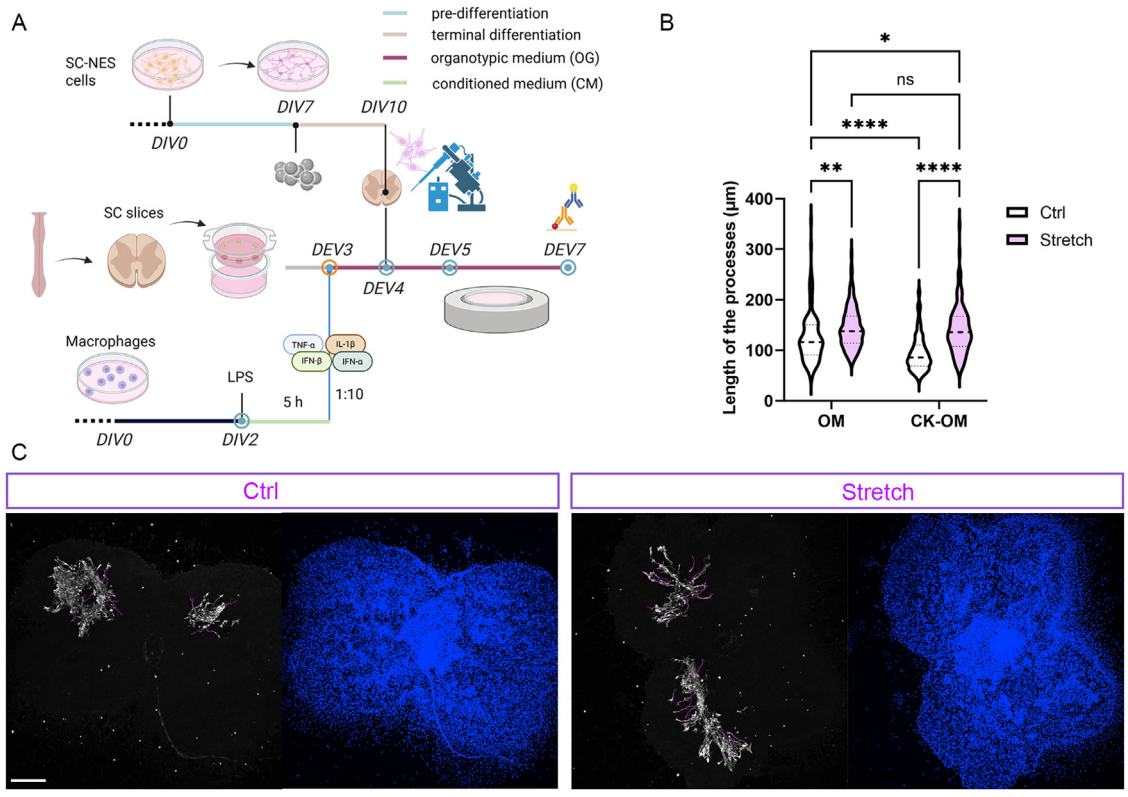

Fig. 7. Elongation of neural processes in SC–NES cells microinjected into control SC slices or exposed to exogenous cytokines. (A) Timeline of the experiment: neuronal progenitors are pre-differentiated, labelled with MNPs at the beginning of terminal differentiation (DIV7), and microinjected at DIV10 in DEV4 SC slices. SC slices are incubated in OG or CK-OG at DEV3. CK-OG consists of 1:10 CM (from LPS-stimulated macrophages) : GM, IL-1β 50 U/ml, TNFα 1000 U/ml, IFNγ 1000 U/ml and IFNα 2000 U/ml. (B) Violin plot of axon length. Two-way ANOVA followed by Tukey's multiple comparison test. Interaction: F (1, 476)=11.50, p = 0.0008. Row (treatment): F (1, 476)=18.60, $p < 0.0001$, Column (stretch): F (1, 476)=68.13, $p < 0.0001$, n = 120 neuronal processes per group. (C) Representative images at DEV7 of cells transplanted in the SC slices, in control or stretched conditions, in CK-OG (grey: human Nestin-staining; blue: Hoechst). Representative images of SC slices in OG are shown in Fig. 6C. Scale bar: 200 µm.

accumulation results in an enrichment of vesicles and organelles within the axon [21,25]. More specifically, we demonstrated that nano-pulling fosters a cross-talk between axonal transport and local translation [21], which is critical for adding new cellular mass and supporting synaptic maturation [23,25].

In this study, we explored whether nano-pulling could modulate axon growth in the presence of chemotaxis, particularly inhibitory cues. To investigate the effect of force under such conditions, we cultured hippocampal neurons on CSPG-coated dishes, as CSPGs are known to inhibit axon growth by various mechanisms, including blocking the function of growth-promoting molecules such as laminin and its receptor integrins, which in turn impairs the generation of endogenous forces and tip advancement [58]. Our results demonstrated that mechanical force application can promote axon growth even in the presence of CSPGs (Fig. 1D, E).

We also examined whether mechanical force could guide axon growth in an inflammatory environment. Isolating cells from the hippocampi of postnatal mice results in a mixed co-culture of neurons and glial cells that support neuron survival [59]. To simulate an inflammatory condition, hippocampal neurons were treated with LPS, which activates the glial cells in the co-culture. As expected, LPS treatment inhibited axon growth, but nano-pulling was able to promote axon growth even in the presence of this inhibition (Fig. 2). Similar results were obtained by treating neurons with a medium enriched with exogenous cytokines (IL-1β, TNF-α, IFN-γ, and IFN-α) added to cytokines released by LPS-stimulated macrophages (Fig. 3). Additionally, even in the presence of SEMA3A, which induces axon shortening by causing growth cone collapse [10], nano-pulling could significantly enhance axon extension (Fig. 4A3). Interestingly, when we exposed the HNs to the combination of these inhibitory signals (CSPGs, LPS, and SEMA3A), we found a substantial reduction in axon length, but nano-pulling was still able to boost axon elongation (Fig. 4B3).

However, it is well known that the chemical environment in neural tissue is highly complex, involving interactions between neuronal and non-neuronal cells and their secreted factors. To address this complexity, we employed organotypic spinal cord cultures, which maintain the original tissue architecture, cell organization, cellular diversity, and extracellular matrix composition of the native organ [60]. One limitation of this model is that spinal cord slices stabilize after a few days *in vitro* (Fig. 5B1, B2), losing the inflammatory response typical of *in vivo* injuries [46]. To simulate an inflammatory condition, spinal cord tissue was treated with LPS. Inflammation was confirmed by microglial activation (Fig. 5E1, E2) and the overexpression of pro-inflammatory cytokines TNFα, IL-6, and IL-1β (Fig. 5B1, B2, D1, D2, D3). MNP-loaded progenitor cells were then microinjected into LPS-pre-treated spinal cord tissue. As expected, LPS treatment caused a significant reduction (approximately 20 %) in the length of neural processes in transplanted NPCs in the control groups (Fig. 6B). However, nano-pulling significantly enhanced the length of neural processes, with no statistically significant difference between LPS-treated and untreated spinal cord slices (Fig. 6B). To mimic features of the inflammatory environment induced by infiltrating macrophages and resident microglia following SCI, we repeated the experiment by incubating SC slices in an organotypic medium enriched with exogenous cytokines (IL-1β, TNF-α, IFN-γ, and IFN-α and cytokines secreted by LPS-stimulated macrophages). Exposure of SC slices to this cytokine-enriched medium led to a significant reduction in the length of neural

projections from transplanted SC–NES cells. Nonetheless, nano-pulling effectively enhanced neural process outgrowth, achieving an elongation rate surpassing that observed under standard culture conditions (Fig. 7B, C).

Together, these findings suggest that even within a complex macromolecular and cellular network, where chemotaxis and intercellular communication plays a critical role, mechanical force can still effectively modulate axon growth. This supports the hypothesis that force can act downstream to chemotaxis [20]. It is well-recognized that many chemical cues can change the endogenous force by inducing cytoskeletal remodelling. Some attractive cues, such as Netrin-1 [61–63], nerve growth factor [64], brain-derived neurotrophic factor [65], and Rac1 signalling pathways [66], promote the reduction of actin retrograde flow, which in turn increases traction force and enhances the contractile force (F_{GC}) generated by the growth cone, stimulating its advance. Conversely, repulsive cues can induce axon retraction by disassembling adhesion points and impairing the generation of contractile force (F_{GC}), as seen with slit-2 [67] and semaphorin 3A [11,68], which cause Cofilin-mediated disassembly of F-actin.

Our data suggest that the generation of an exogenous force, by directly inducing alterations in cytoskeletal tensional homeostasis [21], can be used as a strategy for manipulating axon growth, bypassing certain inhibitory extrinsic factors. However, a limitation of this study is the lack of *in vivo* studies, since cellular and organotypic models retain only part of the complexity of animal studies.

Nano-pulling is emerging as a promising technology with significant translational potential. Various techniques have been explored for generating active forces using cell-stretching substrates [69,70], some of which offer the advantage of remote actuation through mechanisms such as magnetic fields [27,71]. However, a key limitation of these approaches for clinical applications lies in the necessity of implanting these platforms, as they require neurons to grow on stretchable or deformable substrates.

In contrast, nano-pulling presents a non-invasive alternative for generating exogenous forces from within living cells. This approach would leverage the established use of iron oxide nanoparticles and magnetic fields in medicine. However, a major drawback is the requirement for high magnetic field gradients, which, with current technologies, limits the penetration depth to only a few centimeters.

Data and materials accessibility

The authors declare to adhere to the OS principle. Datasets (generated/analyzed) for this study can be found in the ZENODO public database doi: 10.5281/zenodo.14039990.

Declaration of competing interest

The authors declare no conflict of interest.

CRediT authorship contribution statement

Elena Capitanini: Writing – review & editing, Investigation, Data curation. **Laura Talarico:** Writing – review & editing, Investigation. **Sara De Vincentiis:** Writing – review & editing, Investigation, Formal analysis, Data curation. **Chiara Giacomelli:** Investigation, Formal analysis. **Sara Vitolo:** Investigation, Data curation. **Lorenzo Da Palmata:** Investigation, Formal analysis. **Laura Marchetti:** Writing – review & editing, Supervision, Resources, Methodology. **Elisabetta Ferraro:** Writing – review & editing, Supervision, Resources, Methodology, Formal analysis. **Maria Letizia Trincavelli:** Writing – review & editing, Supervision, Methodology. **Vittoria Raffa:** Writing – original draft, Supervision, Project administration, Methodology, Funding acquisition, Formal analysis, Data curation, Conceptualization.

Acknowledgments

The study was partially supported by the Wings for Life Foundation (WFL-IT-16/17 and 20/21), Fondazione Romoli Onlus, and the European Union Next-GenerationEU - National Recovery and Resilience Plan (NRRP) – mission 4 component 2, investment n. 1.4 – CUP N. B83C22003930001 (Tuscany Health Ecosystem – THE", Spoke 8). This manuscript reflects only the authors' views and opinions, neither the European Union nor the European Commission can be considered responsible for them. Stem cell work was performed at Marco Onorati's lab. We would like to thank Alessio Zanelli and Prof. Marco Onorati for the support given with the stem cells, Irene Balloni for PCR analysis, Arianna Votta for the macrophage culture and Paolo Cipolla for the inspiring conversation on inhibitory factors in SCI.

Supplementary materials

Supplementary material associated with this article can be found, in the online version, at doi:10.1016/j.engreg.2025.05.003.

References

[1] H. Tsujioka, T. Yamashita, Neural circuit repair after central nervous system injury, Int. Immunol. 33 (6) (2021) 301–309.
[2] J.W. Fawcett, The struggle to make CNS axons regenerate: why has it been so difficult? Neurochem. Res. 45 (1) (2020) 144–158.
[3] H. Ducuing, T. Gardette, A. Pignata, S. Tauszig-Delamasure, V. Castellani, Commissural axon navigation in the spinal cord: a repertoire of repulsive forces is in command, Semin. Cell Dev. Biol. 85 (2019) 3–12.
[4] S.S. Chambel, C.D. Cruz, Axonal growth inhibitors and their receptors in spinal cord injury: from biology to clinical translation, Neural Regen. Res. 18 (12) (2023) 2573–2581.
[5] M.L. Bennett, A.N. Viaene, What are activated and reactive glia and what is their role in neurodegeneration? Neurobiol. Dis. 148 (2021) 105172.
[6] D.M. Snow, V. Lemmon, D.A. Carrino, A.I. Caplan, J. Silver, Sulfated proteoglycans in astroglial barriers inhibit neurite outgrowth *in vitro*, Exp. Neurol. 109 (1) (1990) 111–130.
[7] K. Sharma, M.E. Selzer, S. Li, Scar-mediated inhibition and CSPG receptors in the CNS, Exp. Neurol. 237 (2) (2012) 370–378.
[8] J. Silver, J.H. Miller, Regeneration beyond the glial scar, Nat. Rev. Neurosci. 5 (2) (2004) 146–156.
[9] A.L. Kolodkin, D.J. Matthes, T.P. O'Connor, N.H. Patel, A. Admon, D. Bentley, C.S. Goodman, Fasciclin IV: sequence, expression, and function during growth cone guidance in the grasshopper embryo, Neuron 9 (5) (1992) 831–845.
[10] Y. Luo, D. Raible, J.A. Raper, Collapsin: a protein in brain that induces the collapse and paralysis of neuronal growth cones, Cell 75 (2) (1993) 217–227.
[11] E.W. Dent, A.M. Barnes, F. Tang, K. Kalil, Netrin-1 and Semaphorin 3A promote or inhibit cortical axon branching, respectively, by reorganization of the cytoskeleton, J. Neurosci. 24 (12) (2004) 3002–3012.
[12] A. Chédotal, J.A. Del Rio, M. Ruiz, Z. He, V. Borrell, F. de Castro, F. Ezan, C.S. Goodman, M. Tessier-Lavigne, C. Sotelo, E. Soriano, Semaphorins III and IV repel hippocampal axons via two distinct receptors, Development 125 (21) (1998) 4313–4323.
[13] S.A. Rabacchi, J.M. Solowska, B. Kruk, Y. Luo, J.A. Raper, D.H. Baird, Collapsin-1/semaphorin-III/D is regulated developmentally in Purkinje cells and collapses pontocerebellar mossy Fiber neuronal growth cones, J. Neurosci. 19 (11) (1999) 4437–4448.
[14] B. Rohm, A. Ottemeyer, M. Lohrum, A.W. Püschel, Plexin/neuropilin complexes mediate repulsion by the axonal guidance signal semaphorin 3A, Mech. Dev. 93 (1–2) (2000) 95–104.
[15] S. Okada, The pathophysiological role of acute inflammation after spinal cord injury, Inflamm. Regen. (2016).
[16] R.J. McKeon, M.J. Jurynec, C.R. Buck, The chondroitin sulfate proteoglycans neurocan and phosphacan are expressed by reactive astrocytes in the chronic CNS glial scar, J. Neurosci. 19 (24) (1999) 10778–10788.
[17] S. Wang, G.M. Smith, M.E. Selzer, S. Li, Emerging molecular therapeutic targets for spinal cord injury, Expert Opin. Ther. Targets 23 (9) (2019) 787–803.
[18] G. Yiu, Z. He, Glial inhibition of CNS axon regeneration, Nat. Rev. Neurosci. 7 (8) (2006) 617–627.
[19] G. Costa, F.F. Ribeiro, A.M. Sebastião, E.M. Muir, S.H. Vaz, Bridging the gap of axonal regeneration in the central nervous system: a state of the art review on central axonal regeneration, Front. Neurosci. 16 (2022).
[20] V. Raffa, Force: a messenger of axon outgrowth, Semin. Cell Dev. Biol. (2022).
[21] A. Falconieri, S. De Vincentiis, V. Cappello, D. Convertino, R. Das, S. Ghignoli, S. Figoli, S. Luin, F. Català-Castro, L. Marchetti, U. Borello, M. Krieg, V. Raffa, Axonal plasticity in response to active forces generated through magnetic nano-pulling, Cell Rep. 42 (1) (2023) 111912.
[22] V. Raffa, F. Falcone, S. De Vincentiis, A. Falconieri, M.P. Calatayud, G.F. Goya, A. Cuschieri, Piconewton mechanical forces promote neurite growth, Biophys. J. 115 (10) (2018) 2026–2033.

[23] S. de Vincentiis, A. Falconieri, M. Mainardi, V. Cappello, V. Scribano, R. Bizzarri, B. Storti, L. Dente, M. Costa, V. Raffa, Extremely low forces induce extreme axon growth, J. Neurosci. (2020).
[24] A. Falconieri, P. Folino, L. Da Palmata, V. Raffa, Nano-pulling stimulates axon regeneration in dorsal root ganglia by inducing stabilization of axonal microtubules and activation of local translation, Front. Mol. Neurosci. 17 (2024).
[25] S. De Vincentiis, M. Baggiani, F. Merighi, V. Cappello, J. Lopane, M. Di Caprio, M. Costa, M. Mainardi, M. Onorati, V. Raffa, Low forces push the maturation of neural precursors into neurons, Small (2023).
[26] S. De Vincentiis, A. Falconieri, F. Mickoleit, V. Cappello, D. Schüler, V. Raffa, Induction of axonal outgrowth in mouse hippocampal neurons via bacterial magnetosomes, Int. J. Mol. Sci. 22 (8) (2021) 4126.
[27] A. Falconieri, N. Taparia, S. De Vincentiis, V. Cappello, N.J. Sniadecki, V. Raffa, Magnetically-actuated microposts stimulate Axon growth, Biophys. J. (2021).
[28] M. Onorati, Z. Li, F. Liu, A.M.M. Sousa, N. Nakagawa, M. Li, M.T. Dell'Anno, F.O. Gulden, S. Pochareddy, A.T.N. Tebbenkamp, W. Han, M. Pletikos, T. Gao, Y. Zhu, C. Bichsel, L. Varela, K. Szigeti-Buck, S. Lisgo, Y. Zhang, A. Testen, X.B. Gao, J. Mlakar, M. Popovic, M. Flamand, S.M. Strittmatter, L.K. Kaczmarek, E.S. Anton, T.L. Horvath, B.D. Lindenbach, N. Sestan, Zika virus disrupts phospho-TBK1 localization and mitosis in Human neuroepithelial stem cells and radial glia, Cell Rep. (2016).
[29] M.T. Dell'Anno, X. Wang, M. Onorati, M. Li, F. Talpo, Y. Sekine, S. Ma, F. Liu, W.B.J. Cafferty, N. Sestan, S.M. Strittmatter, Human neuroepithelial stem cell regional specificity enables spinal cord repair through a relay circuit, Nat. Commun. 9 (1) (2018) 3419.
[30] F. Merighi, S. De Vincentiis, M. Onorati, V. Raffa, Long-term mouse spinal cord organotypic slice culture as a platform for validating cell transplantation in spinal cord injury, J. Vis. Exp. (206) (2024).
[31] J. Jones, A. Estirado, C. Redondo, J. Pacheco-Torres, M.-S. Sirerol-Piquer, J.M. Garcia-Verdugo, S. Martinez, Mesenchymal stem cells improve motor functions and decrease neurodegeneration in ataxic mice, Mol. Ther. 23 (1) (2015) 130–138.
[32] A.R. Coda, S. Anzilotti, F. Boscia, A. Greco, M. Panico, S. Gargiulo, M. Gramanzini, A. Zannetti, S. Albanese, G. Pignataro, L. Annunziato, M. Salvatore, A. Brunetti, P. De Berardinis, M. Quarantelli, G. Palma, S. Pappatà, *In vivo* imaging of CNS microglial activation/macrophage infiltration with combined [18F]DPA-714-PET and SPIO-MRI in a mouse model of relapsing remitting experimental autoimmune encephalomyelitis, Eur. J. Nucl. Med. Mol. Imaging 48 (1) (2021) 40–52.
[33] C. Riggio, M.P. Calatayud, M. Giannaccini, B. Sanz, T.E. Torres, R. Fernández–Pacheco, A. Ripoli, M.R. Ibarra, L. Dente, A. Cuschieri, G.F. Goya, V. Raffa, The orientation of the neuronal growth process can be directed via magnetic nanoparticles under an applied magnetic field, Nanomedicine 10 (7) (2014).
[34] J. Schindelin, I. Arganda-Carreras, E. Frise, V. Kaynig, M. Longair, T. Pietzsch, … A. Cardona, Fiji: an open-source platform for biological-image analysis, Nat. Methods 9 (7) (2012) 676–682.
[35] J. Popko, A. Fernandes, D. Brites, L.M. Lanier, Automated analysis of NeuronJ tracing data, Cytom. Part A 75A (4) (2009) 371–376.
[36] J.R. Siebert, A. Conta Steencken, D.J. Osterhout, Chondroitin sulfate proteoglycans in the nervous system: inhibitors to repair, Biomed. Res. Int. 2014 (2014) 1–15.
[37] A.A.F. da Silva, M.B. Fiadeiro, L.I. Bernardino, C.S.P. Fonseca, G.M.F. Baltazar, A.C.B. Cristóvão, Lipopolysaccharide-induced animal models for neuroinflammation – An overview, J. Neuroimmunol. 387 (2024) 578273.
[38] X. Fu, S.M. Zunich, J.C. O'Connor, A. Kavelaars, R. Dantzer, K.W. Kelley, Central administration of lipopolysaccharide induces depressive-like behavior *in vivo* and activates brain indoleamine 2,3 dioxygenase In murine organotypic hippocampal slice cultures, J. Neuroinflamm. 7 (1) (2010) 43.
[39] D.J. DiSabato, N. Quan, J.P. Godbout, Neuroinflammation: the devil is in the details, J. Neurochem. 139 (S2) (2016) 136–153.
[40] S.S. Shaftel, W.S.T. Griffin, M.K. O'Banion, The role of interleukin-1 in neuroinflammation and Alzheimer disease: an evolving perspective, J. Neuroinflamm. 5 (1) (2008) 7.
[41] K.M. Park, W.J. Bowers, Tumor necrosis factor-alpha mediated signaling in neuronal homeostasis and dysfunction, Cell Signal. 22 (7) (2010) 977–983.
[42] S. Monteiro, S. Roque, F. Marques, M. Correia-Neves, J.J. Cerqueira, Brain interference: revisiting the role of IFNγ in the central nervous system, Prog. Neurobiol. 156 (2017) 149–163.
[43] C. Hoyo-Becerra, Z. Liu, J. Yao, B. Kaltwasser, G. Gerken, D.M. Hermann, J.F. Schlaak, Rapid regulation of depression-associated genes in a new mouse model mimicking interferon-α-related depression in Hepatitis C Virus infection, Mol. Neurobiol. 52 (1) (2015) 318–329.
[44] M. Shelly, L. Cancedda, B.K. Lim, A.T. Popescu, P. Cheng, H. Gao, M. Poo, Semaphorin3A Regulates neuronal polarization by suppressing axon formation and promoting dendrite growth, Neuron 71 (3) (2011) 433–446.
[45] O.N. Hausmann, Post-traumatic inflammation following spinal cord injury, Spinal Cord. 41 (7) (2003).
[46] D.J. Hellenbrand, C.M. Quinn, Z.J. Piper, C.N. Morehouse, J.A. Fixel, A.S. Hanna, Inflammation after spinal cord injury: a review of the critical timeline of signaling cues and cellular infiltration, J. Neuroinflamm. 18 (1) (2021) 284.
[47] G. Panattoni, R. Amoriello, C. Memo, A. Thalhammer, C. Ballerini, L. Ballerini, Diverse inflammatory threats modulate astrocytes Ca2+ signaling via connexin43 hemichannels in organotypic spinal slices, Mol. Brain 14 (1) (2021) 159.
[48] T. Ishijima, K. Nakajima, Inflammatory cytokines tnfα, IL-1β, and IL-6 are induced in endotoxin- stimulated microglia through different signaling cascades, Sci. Prog. 104 (4) (2021).
[49] L. Xu, J. Wang, Y. Ding, L. Wang, Y.-J. Zhu, Current knowledge of microglia in traumatic spinal cord injury, Front. Neurol. 12 (2022).
[50] F. González Ibanez, K. Picard, M. Bordeleau, K. Sharma, K. Bisht, M.-È. Tremblay, Immunofluorescence staining using IBA1 and TMEM119 for microglial density, morphology and peripheral myeloid cell infiltration analysis in mouse brain, J. Vis. Exp. 152 (2019).
[51] X. Gao, Z. Han, C. Huang, H. Lei, G. Li, L. Chen, D. Feng, Z. Zhou, Q. Shi, L. Cheng, X. Zhou, An anti-inflammatory and neuroprotective biomimetic nanoplatform for repairing spinal cord injury, Bioact. Mater. 18 (2022) 569–582.
[52] L.A. Lowery, D. Van Vactor, The trip of the tip: understanding the growth cone machinery, Nat. Rev. Mol. Cell Biol. (2009).
[53] C.S. Barros, S.J. Franco, U. Muller, Extracellular matrix: functions in the nervous system, Cold. Spring Harb. Perspect. Biol. 3 (1) (2011) a005108–a005108.
[54] P. Lamoureux, R.E. Buxbaum, S.R. Heidemann, Direct evidence that growth cones pull, Nature (1989).
[55] M. O'Toole, P. Lamoureux, K.E. Miller, Measurement of subcellular force generation in neurons, Biophys. J. 108 (5) (2015) 1027–1037.
[56] K.E. Miller, D.M. Suter, An integrated cytoskeletal model of neurite outgrowth, Front. Cell Neurosci. 12 (2018).
[57] A. Falconieri, A. Coppini, V. Raffa, Microtubules as a signal hub for axon growth in response to mechanical force, Biol. Chem. 405 (1) (2024) 67–77.
[58] Y. Ohtake, S. Li, Molecular mechanisms of scar-sourced axon growth inhibitors, Brain Res. 1619 (2015) 22–35.
[59] G.M.J. Beaudoin, S.-H. Lee, D. Singh, Y. Yuan, Y.-G. Ng, L.F. Reichardt, J. Arikkath, Culturing pyramidal neurons from the early postnatal mouse hippocampus and cortex, Nat. Protoc. 7 (9) (2012) 1741–1754.
[60] S. Pandamooz, M. Nabiuni, J. Miyan, A. Ahmadiani, L. Dargahi, Organotypic spinal cord culture: a proper platform for the functional screening, Mol. Neurobiol. 53 (7) (2016) 4659–4674.
[61] Z. Qiu, T. Minegishi, D. Aoki, K. Abe, K. Baba, N. Inagaki, Adhesion-clutch between DCC and netrin-1 mediates netrin-1–induced axonal haptotaxis, Front. Mol. Neurosci. 17 (2024).
[62] M. Toriyama, S. Kozawa, Y. Sakumura, N. Inagaki, Conversion of a signal into forces for axon outgrowth through pak1-mediated shootin1 phosphorylation, Curr. Biol. (2013).
[63] T. Shimada, M. Toriyama, K. Uemura, H. Kamiguchi, T. Sugiura, N. Watanabe, N. Inagaki, Shootin1 interacts with actin retrograde flow and L1-CAM to promote axon outgrowth, J. Cell Biol. 181 (5) (2008) 817–829.
[64] S.G. Turney, M. Ahmed, I. Chandrasekar, R.B. Wysolmerski, Z.M. Goeckeler, R.M. Rioux, G.M. Whitesides, P.C. Bridgman, Nerve growth factor stimulates axon outgrowth through negative regulation of growth cone actomyosin restraint of microtubule advance, Mol. Biol. Cell (2016).
[65] J.P. Myers, T.M. Gomez, Focal adhesion kinase promotes integrin adhesion dynamics necessary for chemotropic turning of nerve growth cones, J. Neurosci. (2011).
[66] S. Woo, T.M. Gomez, Rac1 and RhoA promote neurite outgrowth through formation and stabilization of growth cone point contacts, J. Neurosci. (2006).
[67] A. Bellon, A. Iyer, S. Bridi, F.C.Y. Lee, C. Ovando-Vázquez, E. Corradi, S. Longhi, M. Roccuzzo, S. Strohbuecker, S. Naik, P. Sarkies, E. Miska, C. Abreu-Goodger, C.E. Holt, M.-L. Baudet, miR-182 regulates Slit2-mediated axon guidance by modulating the local translation of a specific mRNA, Cell Rep. 18 (5) (2017) 1171–1186.
[68] H. Aizawa, S. Wakatsuki, A. Ishii, K. Moriyama, Y. Sasaki, K. Ohashi, Y. Sekine-Aizawa, A. Sehara-Fujisawa, K. Mizuno, Y. Goshima, I. Yahara, Phosphorylation of cofilin by LIM-kinase is necessary for semaphorin 3A-induced growth cone collapse, Nat. Neurosci. 4 (4) (2001) 367–373.
[69] J. Zhao, F. Meng, J. Qian, Y. Huang, Y. Fan, *In vitro* cell stretching devices and their applications: from cardiomyogenic differentiation to tissue engineering, Med. Nov. Technol. Devices 18 (2023) 100220.
[70] I. Constantinou, E.E. Bastounis, Cell-stretching devices: advances and challenges in biomedical research and live-cell imaging, Trends Biotechnol. 41 (7) (2023) 939–950.
[71] V. Du, N. Luciani, S. Richard, G. Mary, C. Gay, F. Mazuel, M. Reffay, P. Menasché, O. Agbulut, C. Wilhelm, A 3D magnetic tissue stretcher for remote mechanical control of embryonic stem cell differentiation, Nat. Commun. 8 (1) (2017) 400.